Original Research Article

Comprehensive assessment of Ferroresonance and its Effects in Selected Distribution Substations in Nasarawa State, Nigeria

ABSTRACT

Ferroresonance in distribution networks generates harmful harmonics, excessive heating, and potential transformer failures, yet limited research focuses on its impact in Nigerian low-voltage systems. This study examines ferroresonance susceptibility in low-voltage distribution transformers, with an emphasis on core saturation, harmonic distortion, and grading capacitance effects under varied operational conditions across substations in Lafia, Akwanga, and Keffi. By analyzing transformer responses from 50V to 500V and harmonic profiles in Delta (1.12Ω) and Star-Grounded (1.53Ω) configurations, the research highlights transformer design's critical role in ferroresonance resilience. Findings reveal that increasing grading capacitance from 90 pF to 1550 pF substantially elevated peak voltages from 0.420kV to 2.400kV (Lafia), 2.450kV (Akwanga), and 2.540kV (Keffi), and currents from 28A, 26A and 27A to 103A, 118A, and 130A, respectively. Voltage THD similarly rose from 6.5%, 6.3% and 6.7% to 35.5%, 38.2%, and 36.0%, respective; with current THD climbing from 7.8% 7.5% and 7.9% to 40.2%, 44.1%, and 42.3% respectively, indicating varying ferroresonance susceptibility across the substations. Delta configurations show lower ferroresonance risk compared to Star-Grounded types, underscoring optimal winding configuration and capacitance management as key resilience factors. Recommendations include targeted harmonic filtering and precise capacitance management to stabilize transformer operation. Future research should consider broader transformer model diversity, adaptive control systems, and machine learning techniques for enhanced ferroresonance risk assessments.

Keywords: Ferroresonance, distribution transformers, harmonic distortion, grading capacitance, core saturation, transformer resilience.

1. INTRODUCTION

Ferroresonance, although introduced in the early 1900s,was first analytically studied in the 1940s[1]. Major advances came in the 1980s, followed by further research in the 1990s exploring its chaotic, nonlinear behavior [2]. Ferroresonance is a non-linear resonance phenomenon that arises in electrical circuits, particularly when they contain non-linear inductances such as those found in distribution transformers, complex electronic loads, and leakage inductances. Capacitances, like those formed between underground armored cables or other network cables (commonly known as coupling capacitance), alongside a voltage source and low transformer losses, can collectively trigger ferroresonance[3]. When ferroresonance occurs, it introduces abnormal electrical behavior, characterized by erratic voltage fluctuations, harmonic distortions, and sustained oscillations, posing serious threats to the stability and longevity of critical infrastructure, especially transformers.The occurrence of ferroresonance in distribution networks is particularly alarming due to its ability to generate destructive harmonics, cause excessive heating, and even induce catastrophic failures in transformers [4,5]. Audible noise, core saturation, and reduced efficiency are among the physical manifestations, while severe voltage instability can disrupt broader network operations, undermining grid reliability [6]. In Nigeria, where reliable electricity remains a challenge, the adverse effects of ferroresonance further exacerbate the risks to power stability, increasing operational losses and lowering equipment lifespan [7,8,9].

Temiz and Tarkan [10] explored ferroresonance in expanding transmission networks, highlighting its effects, such as oscillations and overvoltages, especially in isolated or star-point networks. Nene [11] investigated Capacitor Coupled Substations (CCS) for rural electrification, focusing on ferroresonance suppression strategies. Gokhale *et al.* [12] studied ferroresonance in single-phase transformers with delta-connected capacitors, proposing load balancing as a

preventive measure. Tovbaev*et al.* [13] analyzed subharmonic oscillations in three-phase circuits, evaluating system stability for converter design. Begmatov [14] examined ferroresonance in three-phase networks, presenting formulas for voltage increase and stable conditions, essential for reliable network operation.Shemshadi andKhorampour[15] investigated ferroresonance between network capacitors and transformer inductance during saturation. Using MATLAB, they explored damping methods such as high resistance, resistors-inductors combinations, and surge arresters to mitigate ferroresonance fluctuations and overvoltage. Zirka*et al.*[16] modeled an isolated neutral network with inductive voltage transformers (VTs) to analyze ferroresonance behavior. Their model was validated against various network capacitances, accurately predicting ferroresonance modes. Full-scale tests showed ferroresonance at around 25Hz for some configurations, while chaotic or no ferroresonance occurred under others. Bini *et al.*[17] used circuit modeling and MATLAB/Simulink to study ferroresonance in transformers. They found that only increasing core loss resistance beyond 0.35MΩ could prevent ferroresonance, while varying capacitance or source voltage merely shifted ferroresonance modes between subharmonic, fundamental, and chaotic states. Olguín-Becerril *et al.*[18] examined ferroresonance in inductive voltage transformers (IVTs), focusing on a 2011 event in Mexico. They simulated the phenomenon using EMTP and proposed damping reactors to mitigate it, demonstrating significant reduction in overvoltages and improved stability in IVT operations. Chen *et al.*[19] investigated ferroresonance in unloaded single-phase transformers connected to a capacitor. They conducted time-domain numerical simulations to analyze harmonic content, revealing that significant capacitor values lead to periodic ferroresonance modes. Core loss resistance was found to effectively damp non-periodic responses.

Despite the well-documented dangers of ferroresonance, there is limited research specifically addressing its occurrence and effects within Nigerian low-voltage distribution systems. Most studies focus on harmonic mitigation strategies in system-level protection schemes, leaving a critical knowledge gap in understanding how ferroresonance manifests and impacts local substations [7,21,22]. Without detailed assessments of ferroresonance in these environments, system operators remain unprepared to tackle its full impact, and existing networks may be more vulnerable to unexpected failures.This work sought to fill that gap by providing a comprehensive assessment of ferroresonance occurrence and its effects in selected distribution substations in Nasarawa State, Nigeria. Given the growing reliance on electrical power systems, understanding these dynamics is essential to preserving network integrity, optimizing performance, and ensuring reliable power delivery in the region. Key objectives are to assess the prevalence of ferroresonance occurrences across selected low-voltage distribution substations in Nasarawa State; as well as to evaluate the effects of ferroresonance on voltage stability, harmonic distortion, and transformer performance within the studied substations.

2. METHODOLOGY

This study adopted a comprehensive analytical approach to model low voltage AC distribution systems under ferroresonance conditions. It integrated nonlinear circuit elements: linear resistor (R), shunt capacitance (C), and both linear (L) and nonlinear inductors (L_{NL}); to analyze voltage and current dynamics. Using Kirchhoff's Voltage Law, the methodology combined simulation via Ferroview software and experimental setups to characterize passive nonlinear elements and predict ferroresonance phenomena, thereby enhancing understanding on the nature of ferroresonance; andits mitigation strategies.

2.1 Modeling the Distribution System under Ferroresonance Conditions

Consider the ferroresonant circuit in Figure 1, which represents a low voltage AC distribution network. The system can be modelled as a linear resistor (R), a shunt capacitance (C) to represent the capacitance of the system; and a series linear inductor (L), as well as a nonlinear inductor (L_{NL}) to represent the iron core.

Thus as reported by Kutija and Pravica[5], the total voltage in the system (V_t) during a ferroresonant event would be given by:

UNDER PEER REVIEW

$$V_t = V_1 + \sum n \left(V_n \cos(n\omega t + \varphi_n)\right) \quad (1)$$

It is expressed as a summation of multiple sinusoidal terms. V_1 is the fundamental voltage component with angular frequency ωt and phase angle φ_1. The summation term ($\sum n$) includes higher-order harmonics ($n > 1$) with respective amplitudes V_n and phase angles φ_n. These higher-order harmonics account for the distortion or non-sinusoidal behavior in the voltage waveform during transient events. Then, the total current in the system (I_t) during the ferroresonant event would be given by:

$$I_t = I_1 + \sum n \left(I_n \cos(n\omega t + \theta_n)\right) \quad (2)$$

It is also expressed as a summation of multiple sinusoidal terms. I_1 is the fundamental current component with angular frequency ωt and phase angle θ_1. The summation term ($\sum n$) includes higher-order harmonics ($n > 1$) with respective amplitudes I_n and phase angles θ_n. These higher-order harmonics account for the distortion or non-sinusoidal behavior in the current waveform during transient events.

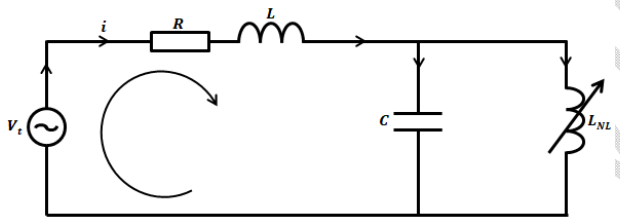

Figure 1: Equivalent Circuit of AC Distribution System under Ferroresonance Condition [5]

It will be assumed that the distribution network includes linear elements like resistance (R) and inductance (L) and nonlinear elements like capacitance (C) and nonlinear inductance (V_{NL}).From Kirchhoff's Voltage Law (KVL), the total voltage applied to the network is the sum of all the voltage drops across the network elements; namely; the voltage drop across the resistance (V_R), the voltage drop across the linear inductance (V_L), the voltage drop across the nonlinear capacitance (V_C), and the voltage drop across the nonlinear inductance (V_{NL}). Thus:

$$V_t = V_R + V_L + V_C + V_{NL} \quad (3)$$

Where

$$V_R = iR; V_L = L\frac{di}{dt}; V_C = \frac{1}{C}\int i(t)dt; \text{ and } V_{NL} = L_{NL}i^2 \cdot \frac{d(i^2)}{dt}$$

So that:

$$V_t = V + \sum n \left(V_n \cos(n\omega t + \varphi_n)\right) = i(t)R + L\frac{di}{dt} + \frac{1}{C}\int i(t)dt + L_{NL}i^2 \cdot \frac{d(i^2)}{dt} \quad (4)$$

Suppose that the current in the network is given by:

$$i(t) = I_1 + \sum n \left(I_n \cos(n\omega t + \theta_n\right) \quad (5)$$

Then, substituting the expression for i(t) into KVL equation (equation 4); and expanding:

$$V + \sum n \left(V_n \cos(n\omega t + \varphi_n)\right) = (I_1 R) + \sum n \left(I_n R \cos(n\omega t + \theta_n)\right) + L\frac{d(I_1)}{dt},$$

UNDER PEER REVIEW

$$V_t = V + \left[I_1 + \sum n\left(I_n cos(n\omega t + \theta_n)\right)\right]R + L\frac{d}{dt}\left[I_1 + \sum n\left(I_n cos(n\omega t + \theta_n)\right)\right] + \frac{1}{C}\int\left[I_1 + \sum n\left(I_n cos(n\omega t + \theta_n)\right)\right] + L_N L\frac{d\left\{\left[I_1 + \sum n\left(I_n cos(n\omega t + \theta_n)\right)\right]^2\right\}}{dt} \quad (6)$$

The derivative of the cosine term can be simplified using the chain rule:

$$\frac{d(cos(n\omega t + \theta_n)}{dt} = -n\omega \times sin(n\omega t + \theta_n) \quad (7)$$

After integrating and differentiating:

$$V + \sum n\left(V_n cos(n\omega t + \varphi_n)\right) = (I_1 R) + \sum n\left(I_n R cos(n\omega t + \theta_n)\right) + L\frac{d(I_1)}{dt} - \sum n\left(n\omega L I_n sin(n\omega t + \theta_n)\right) + \left(\frac{1}{C}\right) \times \left(I_1 t + \sum n\left(I_n\left(\frac{1}{n\omega}\right)\sin(n\omega t + \theta_n\right) + L_{NL}\left(I_1^2 + 2I_1\sum n\left(I_n \cos(n\omega t + \theta_n)\right)\right) + \sum n\left(I_n^2 cos^2(n\omega t + \theta_n)\right) \times 2\, I_1\frac{d(I_1)}{dt} + 2\sum n\left(I_n \cos(n\omega t + \theta_n)\right)\frac{d(I_n)}{dt} \quad (8)$$

Since the expression contains multiple harmonic terms with different frequencies, we can separate them into individual equations for each harmonic component of the voltage and current.The final expression will depend on the specific harmonic components present in the system and the nonlinear characteristics of the inductance. The coefficients (I_1, I_n, V_n, θ_n, φ_n) will depend on the particular network configuration and the behavior of the nonlinear elements. The nonlinear inductance term (L_{NL}) represents the contribution of the nonlinear inductance to the overall system behavior.

The equation can be further analyzed and simplified based on specific system conditions and assumptions. So it is possible to make some hypothetical assumptions to simplify the expression:

Assumptions: We consider a single harmonic component ($n = 1$) for both voltage and current. This means we assume only one frequency (ω) is present in the system, and the other harmonic components are negligible. The nonlinear inductance term (L_{NL}) is constant and can be represented by a single parameter (L_{NL}).With these assumptions, the equation becomes:

$$V_t = V + V_1 cos(\omega t + \varphi_1) = I_1 R + L\frac{d(I_1)}{dt} + \left(\frac{1}{C}\right)\int I_1 dt + L_{NL} I_1^2\frac{d(I_1^2)}{dt} \quad (9)$$

So that for 'n' number of harmonics:

$$V_t = V + \sum n\left(V_n cos(n\omega t + \varphi_n)\right) = iR + L\frac{di}{dt} + \frac{1}{C}\int i(t)dt + L_{NL} i^2 \cdot \frac{d(i^2)}{dt} \quad (10)$$

This developed model was employed in an experimental setup usingFerroview2.0 to simulate the behavior of low-voltage distribution networks and identify potential ferroresonance risks. Key factors include resonant frequencies matching harmonic components, switching events causing transient fluctuations, and nonlinear loads generating harmonic distortion. The model also considers faults that excite resonant frequencies and transformer configurations (e.g., parallel operation, delta-wye connection) that may lead to ferroresonance, as highlighted by Majka and Klimas [22].

2.2 Modeling of the Passive Nonlinear Elements within Electrical Distribution Systems

In this section, the characterization and prediction of ferroresonance phenomena in low voltage distribution systems are closely linked to the characterization of passive nonlinear elements (PNE) within electrical distribution systems [23]. These PNE include nonlinear inductances (NI) (including the studied transformer and associated system inductances), capacitances, and resistances (representing various forms

UNDER PEER REVIEW

of system resistances). Developing a generalized model for these elements and determining their equivalent parameters is of utmost importance in both theoretical and practical contexts. After a model for the analysis of a distribution system has been formulated, what remains is to characterize each of the various elements captured by the developed model equation.One crucial aspect of modeling these nonlinear elements is capturing the relationship between magnetic induction (b) and field strength (h), taking into account surface effects and substance dynamics. Understanding and accurately modeling this relationship is vital for analyzing and predicting the behavior of ferroresonance phenomena in low voltage distribution systems. It allows for the characterization of magnetic behavior and its impact on system dynamics, facilitating the identification and mitigation of potential ferroresonance issues. This relationship, according to Begmatov*et al.*[23] can be mathematically represented by developing equations (10) through (16):

$$b = F_1\left(h, \frac{dh}{dt}, \dots, \frac{db}{dt}, \frac{d^2b}{dt^2}, \dots\right) \qquad (11)$$

In practical scenarios, the current (i) in a nonlinear inductance (NI) often depends on the flux linkage (ψ). In such cases, neglecting higher-order derivatives, equation (11) can be simplified to the following form:

$$i = F_2\left(\psi, \psi^n; \frac{d\psi}{dt}, \frac{d^2\psi}{dt^2} \dots\right) \qquad (12)$$

Equation (12) in the general case describes the equivalent circuit of the Nonlinear Inductances, which is its generalized model as illustrated in Figure 2. If we assume that the equivalent parameters L_s (leakage inductances in the system; such as transformers), $C_э$ (system capacitances), and $g_э$ (equivalent active conductivity of the system representing all resistance elements in the distribution system that account for the damping effect within the system) in this circuit are constant, then we obtain equation (13):

$$i = C_э \frac{d^2\psi}{dt^2} + g_э \frac{d\psi}{dt} a\psi + b\psi^n + \frac{\psi}{L_S} \qquad (13)$$

Where $b\psi^n$ is the approximation of the Weber-ampere characteristic of the system, obtained on the basis of the magnetization curve $B = f(H)$, $C_э$is the equivalent electromagnetic capacitance of the system, $g_э$is the equivalent active conductivity of the system; $L_S$is the leakage inductance of the system. Assuming that the voltage across the inductor is described by $v = V_m \cos \omega t$, Then:

$$\begin{cases} i_S = \frac{\psi}{L_S} = a\psi;\ 2nd\ derivative\ of\ a = \frac{1}{L_S}; \\ \psi = \frac{Vm}{\omega} \sin \omega t = \Psi_m \sin \omega t; \\ i_C = C_э \frac{d^2\psi}{dt^2} = -\omega^2 C_э \Psi_m \sin \omega t = -I_{Cm} \sin \omega t\,; \\ i_g = \frac{1}{R_э} \cdot \frac{d\psi}{dt} = \frac{\Psi_m \omega}{R_э} \cos \omega t = I_{gm} \cos \omega t. \end{cases} \qquad (14)$$

From (13), taking into account the adopted approximation, it then follows that:

$$\begin{cases} i_C = \frac{I_{cm}}{\Psi_m} \psi; \\ i_g = \pm \frac{I_{gm}}{\Psi_m} \sqrt{\Psi_m^2 - \psi^2}; \\ i_L = a\psi + b\psi^n, \end{cases} \qquad (15)$$

Where $i_L' = i_S + i_L$. Thus from (15):

$$i = \left(a - \frac{I_{cm}}{\Psi_m}\right)\psi + b\psi^n \pm \frac{I_{gm}}{\Psi_m} \sqrt{\Psi_m^2 - \psi^2} \qquad (16)$$

UNDER PEER REVIEW

Now an analysis of ferroresonance in the low voltage distribution system transformer can be performed by modifying the equivalent circuit of Figure 2 with distribution transformer (Electro-Magnetic Transformers or EMTs) and network capacitances using the generalized model of nonlinear inductance (NI).

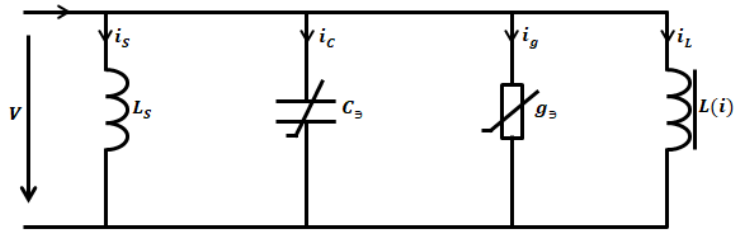

Figure 2: Generalized Nonlinear Inductance Electromagnetic Transformer (NI-EMT) Model [23]

On the basis of equation (16), it is possible to construct the dynamic characteristic of the Nonlinear Inductance model, which is in fact; its hysteresis loop (shown in Figure 3).Assuming that Σ_g, Σ_C and L_0account for all existing system nonlinear components, the combined contribution of which; with the right conditions, give rise to the occurrence of ferroresonance; and that these remain constant, then equation (13) can be approximated thus:

$$i = \sum C\frac{d^2}{dt^2} + \sum g\frac{d\psi}{dt} + a\psi + b\psi^n + \frac{\psi}{L_0} \qquad (17)$$

Where $\sum C$ represents the total electromagnetic capacitance of the distribution transformer, $\sum g = \frac{1}{\sum R}$is the equivalent active conductivity of the system (representing all resistance elements in the transformer that account for the damping effect within the system), L_0represents the equivalent leakage inductances (representing all the nonlinear inductive circuits within the system) and $a\psi + b\psi^n = i_{\mu H}$ = approximation of the Wb – Amp xtics.

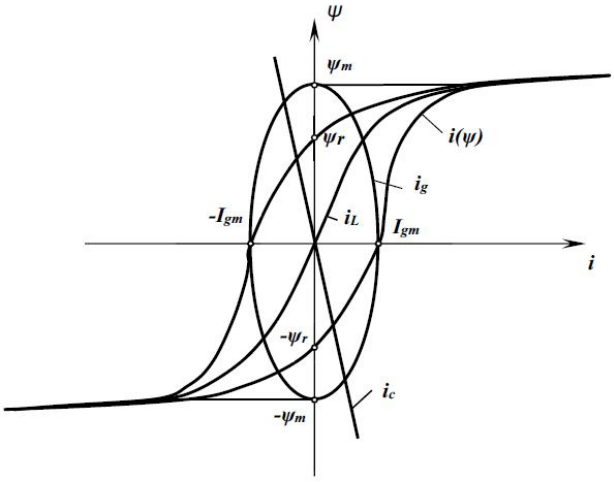

Figure 3: Dynamic Hysteresis Loop for the Nonlinear Inductance Model [23]

Equation (17) can be used to describe a modification of the equivalent circuit of Figure 2; as illustrated by Figure 4.Considering that the voltage in Figure 4 is $v = V_m \cos \omega t$, and taking into account; the Hoshimov*et al.*[24] adopted approximation of the Weber-ampere characteristic of NI EMT model, we write:

UNDER PEER REVIEW

$$\begin{cases} i\sum C = \frac{I_{cm}}{\Psi_m}\psi; \\ i\sum g = \pm\frac{I_{gm}}{\Psi_m}\sqrt{\Psi_m^2 - \psi^2}; \\ i_{\mu H} = a\psi + b\psi^n, \end{cases} \quad (18)$$

From (3.16), we obtain:

$$i = i_{\sum C} + i_{\sum g} + i_{\mu H} = \left(a - \frac{I_{cm}}{\Psi_m}\right)\psi + b\psi^n \pm \frac{I_{gm}}{\Psi_m}\sqrt{\Psi_m^2 - \psi^2} \quad (19)$$

On the basis of equation (19), it is possible to construct a dynamic characteristic of a distribution transformer, which would be identical to the dynamic loop of nonlinear inductance hysteresis shown in Figure 3.

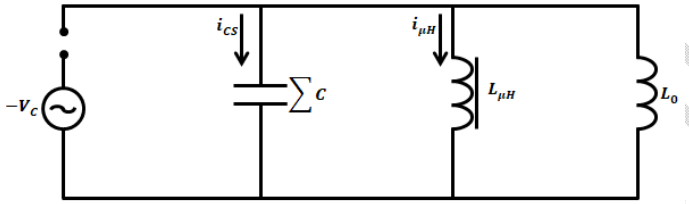

Figure 4: Equivalent Circuit of the transformer with Nonlinear Inductances (distribution transformers and other system inductances), Resistive Loads and Capacitances [23]

The total active conductivity of the nonlinear inductance (NI) in the transformer is influenced by the dynamic coercive force (H_{cd}) and time-varying magnetic induction ($B = B_m \sin\omega t$) in the core [24]. These factors determine the transformer's ability to conduct current efficiently. Thus:

$$H_{cd} = H_C + 0.125\omega\sigma d^2 B_S\sqrt{2\varepsilon - 1} \quad (20)$$

Where Dynamic Coercive Force (H_{cd}) is Magnetic field strength needed to demagnetize the core material during dynamic magnetization [23].Magnetic Core Material (μ_f) is the material used for the core of the transformer, typically made of ferromagnetic material like iron or silicon steel. Induction (in this context, $B = B_m \sin(\omega t)$) represents the time-varying magnetic induction (B) in the core of the transformer. H_C is the static coercive force, representing the magnetic field strength required to reduce the magnetic induction (B) to zero under static conditions.ω is the angular frequency of the alternating current (AC) flowing through the transformer.d is the thickness of the ferromagnetic material, which is used to construct the core of the transformer.σ is the conductivity of the core material expressed as ($\sigma = \frac{B_m}{B_S}$).B_S is the saturation magnetic induction, representing the maximum magnetic induction that the core material can sustain under given operating conditions.ε is the coefficient of the dynamic hysteresis loop, representing the dynamic behavior of the ferromagnetic material during magnetization.The dynamic coercive force (H_{cd}) combines the effects of static coercive force (H_C) and dynamic magnetization, influenced by the term $(0.125\omega\sigma d^2 B_S\sqrt{2\varepsilon - 1})$. This term accounts for core material thickness (d), conductivity (σ), AC frequency (ω), saturation magnetic induction (B_S), and dynamic hysteresis loop coefficient (ε). These factors affect the core's ability to sustain magnetization, crucial for transformer performance during operation [23, 24].If 'V' is the voltage applied to the transformer, and '$\sum R$' the total resistance in the circuit, then:

$$\frac{V}{\sum R} = \frac{H_{cd}l}{w} = \frac{l}{w}\left(H_C + 0.125\omega\sigma d^2 B_S\sqrt{2\varepsilon - 1}\right) \quad (21)$$

UNDER PEER REVIEW

Where l; is the length of the core, and; the term $\frac{l}{w}$ refers to the ratio of the length (l) of the core to the width (w) of the core. To get the equivalent active resistance of the nonlinear electromagnetic transformer (NI EMT) voltage:

$$\sum R = \frac{Vw}{l\left(H_C + 0.125\omega\sigma d^2 B_S\sqrt{2\varepsilon - 1}\right)} = \frac{\omega w^2 SB}{l\left(H_C + 0.125\omega\sigma d^2 B_S\sqrt{2\varepsilon - 1}\right)} \qquad (22)$$

Where 'w' is the width of the core; 'S' is the cross-sectional area of the magnetic core; and 'B' represents the magnetic induction or magnetic flux density in the magnetic core.Using equation (18) the equivalent parameters $\sum$ C and L_0 for the transformer can then be determined [23, 25]:

$$\sum C = \frac{a\Psi_r + b\Psi_r^n - \frac{1}{R}\sqrt{\left(V_m^2 - \Psi_r^2\omega^2\right)}}{\omega^2\psi_r} = \frac{a\Psi_r + b\Psi_r^n - \frac{\omega}{R}\sqrt{\left(\Psi_m^2 - \Psi_r^2\right)}}{\omega^2\psi_r} \qquad (23)$$

And;

$$L_0 = \frac{\psi_r}{\frac{1}{\psi_m}\left(I_{cm}\psi_r + I_{gm}\sqrt{\psi_m^2 - \psi_r^2}\right) - b\psi_r^n} \qquad (24)$$

Considering that the flux linkage in the dynamic characteristic of NI EMT is given by $\psi = \psi_m \sin\omega t$; and taking into account that $i_{\mu H} = a\psi + b\psi^n$, then for the current in the ascending branch of the hysteresis loop in Figure 4, Hoshimov *et al.*[24] posit that the following expression holds:

$$i = I_{1m}\sin(\omega t + a) - \frac{b}{4}\Psi_m^n \sin 3\omega t \qquad (25)$$

Where I_{1m} is the maximum value of the current in the ascending branch of the hysteresis loop.a is a phase angle related to the system parameters (I_{gm}, $a\Psi_m + (\frac{3}{4})b\Psi_m^n - I_{cm}$).b is a coefficient related to the nonlinear behavior of the system.Ψ_m^n is the nth power of the maximum magnetic flux linkage ψ_m.
And:

$$I_{1M} = \sqrt{\left(a\Psi_m + \frac{3}{4}b\Psi_m^n - I_{cm}\right)^2 + I_{gm}^2} \qquad (26)$$

Where I_{gm} is the amplitude of the Gauss random noise in the system.I_{cm} is the minimum value of the current in the descending branch of the hysteresis loop.And:

$$a = arctg\frac{I_{gm}}{a\Psi_m + \frac{3}{4}b\Psi_m^n - I_{cm}} \qquad (27)$$

If the instantaneous power in the nonlinear transformer equals:

$$p = V_m I_{1m}\cos\omega t \sin(\omega t + a) - \frac{b}{4}V_m\Psi_m^n; \qquad (28)$$

Then, as reported by Hoshimov*et al.*[24] we have:

$$p = \frac{w^2S^2\omega^2B_m^2}{2}\cdot\frac{1}{\sum R} = 2\pi^2 w^2 S^2 f^2 \sigma B_m^2 \qquad (29)$$

Where:

UNDER PEER REVIEW

$$\sum \sigma = \frac{1}{\sum R} \qquad (30)$$

2.3 Occurrence and Effects of Ferroresonance in Low Voltage Distribution Networks

This section presents case studies of ferroresonance in low voltage environments by combining substation parameter measurements, experimental tests, and simulations. Using advanced modeling tools, scenarios were created by opening switches between buses A and B, allowing a resonant circuit through grading capacitances. Disconnecting the baseline transformer (SST2) altered the capacitance-inductance balance, inducing ferroresonance. Parametric studies varied grading capacitances, transformer characteristics, filters, and load parameters. Incremental capacitance changes and switching sequences were analyzed to assess transient effects. The study identified key parameters influencing ferroresonance impact and optimal configurations to reduce losses and improve efficiency. The in-situ measurement set-up for all collected substation data is illustrated in Figure 5, while Table 1 presents the measured data from the respective substations.

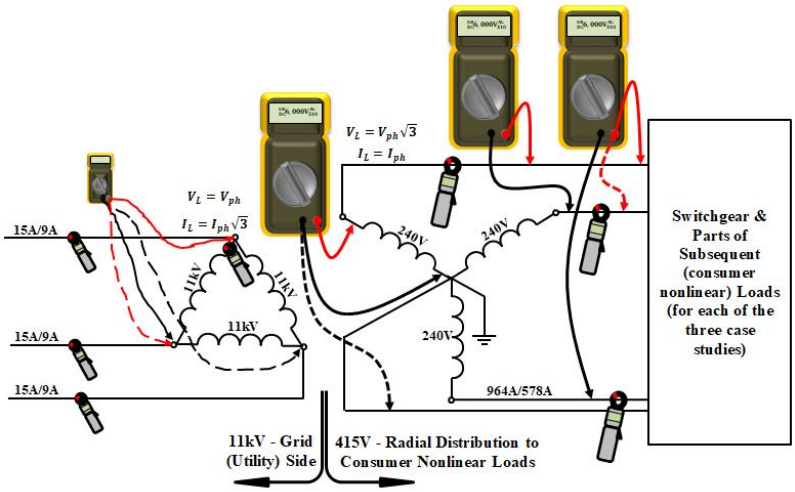

Figure 5: On-site Measurement Set-up for the Substation Data used for Ferroresonance Investigations

2.4 The Experimental Set-Up for Studying Key Parameters Influencing Ferroresonance Occurrence

The experimental setup was carefully designed to replicate operational conditions observed in typical distribution transformers under potential ferroresonance scenarios. The 30kVA transformer, chosen for its prevalence in local distribution networks, was connected to a variable AC voltage source to enable stepwise adjustments in applied voltage and frequency. This setup allowed for controlled simulation of overvoltage conditions, typical in ferroresonance.

Plate 1: Experimental Set-up for Key Design Parameters that Influence Impact of Ferroresonance on the Transformer

UNDER PEER REVIEW

2.4.1 Choice of Measurement Instruments

Each instrument used in this setup was selected based on accuracy and sensitivity to parameters directly influencing ferroresonance, ensuring reliable data collection. For example, the oscilloscope and power quality analyzer were selected for their high precision in capturing voltage and current waveforms, essential for analyzing harmonic distortions and core saturation. An LCR meter was specifically chosen to accurately measure inductance and capacitance, given these parameters' influence on resonance characteristics.

Table 1: Measured Data for the Respective Substations

Component/Element	Parameter	Lafia Substation	Akwanga Substation	Keffi Substation
Power Source	Line-to-Line Voltage	11kV	11kV	11kV
	Frequency	50Hz	50Hz	50Hz
	Per Phase Short-Circuit Impedance	0.018Ω + j0.360Ω	0.0185Ω + j0.365Ω	0.0172Ω + j0.356Ω
Bus-line B1-B2	Line Filter 1 Resistance (R)	0.185Ω	0.190Ω	0.180Ω
	Line Filter 1 Reactance (X)	1.405Ω	1.410Ω	1.400Ω
	Line Filter 1 Capacitance (C)	0.081µF	0.082µF	0.080µF
	Line Filter 2 Resistance (R)	0.160Ω	0.165Ω	0.155Ω
	Line Filter 2 Reactance (X)	1.410Ω	1.415Ω	1.405Ω
	Line Filter 2 Capacitance (C)	0.112µF	0.114µF	0.110µF
Bus-lines Interconnections	Series Capacitance (CY)	0.0000930µF	0.0000935µF	0.0000925µF
	Parallel Capacitance (CL)	0.000450µF	0.000455µF	0.000445µF
Circuit Breaker	Grading Capacitance (C_g)	Variable	Variable	Variable
Bus-line A1-A2	Stray Capacitance (C_s)	Variable	Variable	Variable
Voltage Transformers (VTs)	Type	Dyn0	Dyn0	DNyn0
	Rated Voltages	11/0.415kV	11/0.415kV	11/0.415kV
	Short-Circuit Test (R_(sh,1w))	7.51Ω	7.52Ω	7.50Ω
	Short-Circuit Test (X_(sh,1w))	0.0025Ω	0.0030Ω	0.002Ω
	Short-Circuit Test (R_(sh,2w))	0.0455Ω	0.0460Ω	0.0450Ω
	Short-Circuit Test (X_(sh,2w))	0.1605Ω	0.1610Ω	0.1600Ω
	No Load Test Current	0.00485A	0.00490A	0.00480A
	No Load Test Flux	0.385W^(-T)	0.390W^(-T)	0.380W^(-T)
	Core Loss Resistance (R_m)	9.53MΩ	9.54MΩ	9.50MΩ
Substation Transformer (SST)	Type	DNy0	DNy0	DNy0
	Grounding Impedance	2.55Ω	2.6Ω	2.5Ω
	Rated Voltages	11/0.415kV	11/0.415kV	11/0.415kV
	Short-Circuit Test (R_(sh,1w))	12.6Ω	12.7Ω	12.5Ω
	Short-Circuit Test (X_(sh,1w))	326Ω	327Ω	325Ω
	Short-Circuit Test (R_(sh,2w))	0.0016Ω	0.0017Ω	0.0015Ω
	Short-Circuit Test (X_(sh,2w))	0.1105Ω	0.1110Ω	0.1100Ω
	No Load Test Current	0.0251A	0.0252A	0.0250A
	No Load Test Flux	0.0455W^(-T)	0.0460W^(-T)	0.0450W^(-T)
	Core Loss Resistance (R_m)	3.12MΩ	3.13MΩ	3.10MΩ
Load	Resistance (R)	166.0Ω	197.0Ω	265.0Ω
	Reactance (X)	0.275Ω	0.280Ω	0.270Ω

As presented in Table 1,the 11kV voltage and 50Hz frequency were measured using a high-voltage voltmeter and frequency meter. Short-circuit impedance was determined via an impedance analyzer. Resistance, reactance, and capacitance for Line Filters 1 and 2 were measured with an LCR meter, while bus-line capacitances were obtained using a network analyzer. Key transformer parameters, including short-circuit tests, no-load currents, and core losses, were recorded using an impedance analyzer, oscilloscope, and power quality analyzer. Load resistance/reactance values for the Lafia, Akwanga, and Keffi Substations were 166.0Ω/0.275Ω, 197.0Ω/0.280Ω, and 265.0Ω/0.270Ω, respectively.

UNDER PEER REVIEW

2.5 Core Saturation Characteristics Measurement: A variable AC voltage source was connected to the 30kVA transformer's primary winding. Voltage, current, and inductance were monitored using tools like an oscilloscope and LCR meter as the supply voltage increased from 0V to 500V. This range allowed us to capture the B-H curve up to high flux densities, directly correlating with ferroresonance scenarios.A B-H curve tracer identified significant hysteresis and core losses at high flux densities.The B-H curve tracer used was selected to accurately measure hysteresis losses at incremental flux densities, enhancing reproducibility by allowing other researchers to match the test conditions precisely.

2.6 Winding Configuration Studies: The transformer, arranged in a Delta-Star configuration, had its impedance characteristics analyzed using an impedance analyzer.The Delta-Star configuration was selected based on its prevalence in local distribution setups and its documented resilience to ferroresonance. Impedance analysis of this configuration, conducted using an impedance analyzer, allowed us to evaluate how this configuration's unique impedance characteristics influence ferroresonance susceptibility.

2.7 Nonlinear Inductance Studies: A distorted waveform with 5% 3rd and 3% 5th harmonics was applied, and harmonic currents were measured using FFT analysis, revealing nonlinear inductance behavior.This injected harmonic content was chosen based on typical harmonic levels in distribution networks influenced by non-linear loads.

2.8 Inductance Measurement: An LCR meter was used to measure inductance at different current levels, showing the transformer's non-linear behavior.

2.9 Capacitance Measurements: Capacitance between the windings, ground, and series capacitance was measured using a capacitance meter and network analyzer.The applied values are critical for modeling ferroresonance susceptibility, as they reflect real substation conditions.

2.10 Load Impact Studies: The transformer was tested with resistive (10kW), inductive, and capacitive loads (10kVAR), and responses were monitored via voltage and current measurementsreflecting the load diversity found in local substations.

2.11 System Voltage and Frequency Impact Studies: Nominal system voltage (230V) and frequency (50Hz) were applied to assess transformer performance under rated conditions, using an oscilloscope and power quality analyzer.

3. RESULTS

The measurements of core saturation (Table 2) show that at low voltages (50V, 100V), magnetizing current and losses are minimal, indicating low ferroresonance risks. However, at higher voltages (200V, 300V); magnetizing current rises, indicating core saturation. At 400V and 500V, saturation deepens, significantly increasing risk due to elevated magnetizing currents and core losses.

Table 2: Measured Core Saturation Characteristics

Applied Voltage (V)	Magnetizing Current (A)	Hysteresis Losses (W/kg)	Core Losses (W/kg)
0	0	0	0
50	0.1	0.5	1.0
100	0.3	1.0	2.5
200	1.0	2.0	5.0
300	2.5	3.5	8.0
400	2.7	5.0	11.0
500	4.5	6.5	15.0

UNDER PEER REVIEW

Table 3 illustrates the impact of winding configurations on transformer impedance. The Delta configuration has the lowest impedance (1.12Ω), indicating a lower risk of ferroresonance. The Star configuration (1.39Ω) has a moderate risk, while Delta-Grounded (1.27Ω) and Star-Grounded (1.53Ω) configurations have higher impedances, suggesting increased stability but greater potential for ferroresonance under stress.

Table 3: Measured Winding Configuration Impedances

Configuration	Resistance (Ω)	Reactance (Ω)	Impedance (Ω)
Delta	0.5	1.0	1.12
Star	0.7	1.2	1.39
Delta-Grounded	0.6	1.1	1.27
Star-Grounded	0.8	1.3	1.53

Table 4 reveals harmonic currents and voltages across harmonic orders. The 3rd harmonic exhibits the highest current (0.5A) and voltage (15V), significantly influencing the transformer's non-linear inductance behavior, potentially triggering ferroresonance. As harmonic order increases, currents and voltages decrease, emphasizing the need to manage lower-order harmonics to mitigate ferroresonance risks.

Table 4: Measured Nonlinear Inductance

Harmonic Order	Harmonic Current (A)	Harmonic Voltage (V)
3rd	0.5	15
5th	0.3	10
7th	0.2	8
9th	0.1	5
11th	0.05	3

Table 5 presents transformer inductance at varying currents. At low currents (0.1A), inductance is high (150mH), sustaining resonant conditions. As current rises to 1.0A, inductance decreases, reducing reactiveness and ferroresonance risk. However, high initial inductance at low currents could initiate ferroresonance, decaying as current increases.

Table 5: Measured Inductance

Current (A)	Inductance (mH)
0.1	150
0.5	140
1.0	130
2.0	120
3.0	110
4.0	100

Table 6 outlines capacitance values critical for ferroresonance risk. Capacitance between windings (50nF) and between windings and ground (30nF) indicates a reactive component that can interact with inductive elements. Series capacitance (20nF) further contributes to potential resonance. Managing these capacitances is essential to mitigate ferroresonance risks.

Table 6: Measured Capacitance

Measurement Type	Capacitance (nF)
Between Windings	50
Between Windings and Ground	30
Series Capacitance	20

UNDER PEER REVIEW

Table 7 examines load types' effects on transformers. Resistive loads ensure stable operation with low ferroresonance risk. Inductive loads cause slight delays in current response, possibly triggering ferroresonance. Capacitive loads ensure voltage stability but increase losses, heightening ferroresonance likelihood. Load type significantly impacts transformer stability and susceptibility to ferroresonance.

Table 7: Measured Parameters for Load Impact

Load Type	Voltage (V)	Current (A)	Power Factor	Observations
Resistive	230	43.5	1.0	Stable operation, minimal losses
Inductive	230	43.5	0.8	Slight delay in current response
Capacitive	230	43.5	0.9	Voltage stability, higher losses

Table 8 assesses voltage and frequency variations on transformer performance. Under nominal conditions (230V, 50Hz), stability is maintained. Overvoltage (253V, 50Hz) raises core losses, increasing ferroresonance risk. Undervoltage (207V, 50Hz) reduces efficiency, potentially destabilizing the system. Frequency drops (230V, 45Hz) increase magnetizing current, raising ferroresonance potential, while frequency rise (230V, 55Hz) lowers risk, emphasizing the importance of nominal conditions.

Table 8: Measured Impact of System Voltage and Frequency

Condition	Voltage (V)	Frequency (Hz)	Observations
Nominal	230	50	Stable operation, nominal performance
Overvoltage	253	50	Increased core losses, potential overheating
Undervoltage	207	50	Reduced efficiency, potential underperformance
Frequency Drop	230	45	Increased magnetizing current, potential saturation
Frequency Rise	230	55	Reduced core losses, stable operation

3.1 Effect of Variation in Grading Capacitance

This simulationanalyzed occurrences and effects of ferroresonance within low voltage distribution systems by varying the grading capacitor (Cg) values for the studied substations (Crown Luxury Hotel substation in Lafia, Central Primary School substation in Akwanga, and Keffi. The goal was to determine the range within which ferroresonance is most likely to occur. The system was energized by an AC source with a line-to-line peak voltage of 0.40kV at 50 Hz. A time-controlled switch was engaged, closing at 0 seconds and opening at 0.035 seconds.The simulation results, presented in Table 9, cover the selected substations—Lafia, Akwanga, and Keffi. This table demonstrates the effects of varying the grading capacitance values on the peak voltage and current recorded at the Voltage Transformers (VTs) before and after the switch operation. Additionally, Figure 6 illustrates the baseline transformer voltage dynamic responses at different grading capacitance levels—90pF, 1350pF, and 1550pF—for each substation, highlighting scenarios where ferroresonance either occurred or did not. The associated current dynamics are presented in Figure 7.

Table 9: Effects of Varying the Grading Capacitance

C_g (pF)	**Substation**	**Peak Voltage Before Switch Opening (kV)**	**Peak Voltage After Switch Opening (kV)**	**Peak Current Before Switch Opening (A)**	**Peak Current After Switch Opening (A)**	**Voltage THD (%)**	**Current THD (%)**
90	Lafia Substation	0.415	0.420	27	28	6.5%	7.8%
280	Lafia Substation	0.415	0.450	27	39	9.1%	11.4%
700	Lafia Substation	0.415	0.600	27	52	14.8%	17.2%
1350	Lafia Substation	0.415	1.850	27	71	28.3%	31.9%
1550	Lafia Substation	0.415	2.400	27	103	35.5%	40.2%
90	Akwanga Subst.	0.415	0.420	27	26	6.3%	7.5%
280	Akwanga Subst.	0.415	0.450	27	36	8.9%	10.8%

UNDER PEER REVIEW

700	Akwanga Subst.	0.415	0.720	27	49	16.1%	18.7%
1350	Akwanga Subst.	0.415	1.950	27	67	30.5%	34.3%
1550	Akwanga Subst.	0.415	2.450	27	118	38.2%	44.1%
90	Keffi Substation	0.415	0.420	27	27	6.7%	7.9%
280	Keffi Substation	0.415	0.430	27	37	8.7%	11.1%
700	Keffi Substation	0.415	0.700	27	48	15.6%	18.1%
1350	Keffi Substation	0.415	1.800	27	79	27.4%	32.0%
1550	Keffi Substation	0.415	2.540	27	130	36.0%	42.3%

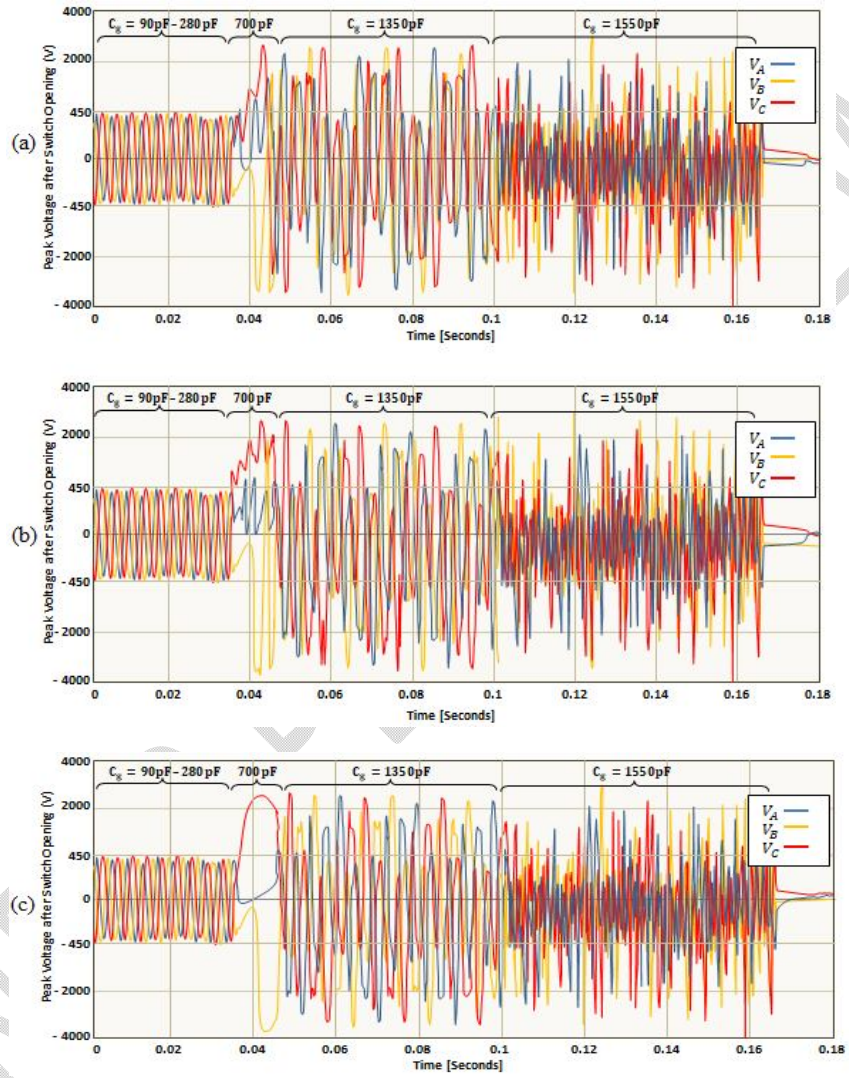

Figure 6: Baseline Transformer Voltage Responses at Various Grading Capacitance Levels for all the Substations; (a) Lafia; (b) Akwanga; and (c) Keffi

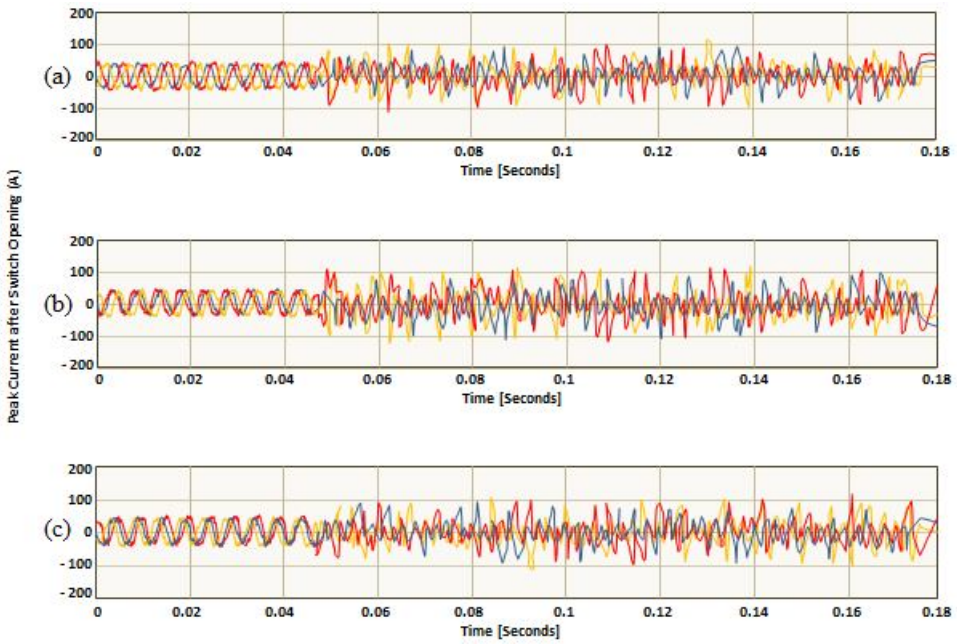

Figure 7: Baseline Transformer Current Responses at Various Grading Capacitance Levels for all the Substations; (a) Lafia; (b) Akwanga; and (c) Keffi

3.2 Load Impact Analysis

Further analysis involved varying load parameters to observe their impact on peak voltage and current during the switching operation. Baseline values were set with resistance (R) at 310.0Ω and reactance (X) at 0.35Ω. The findings, shown in Table 10, revealed that reducing the resistance and reactance increased both the likelihood and severity of ferroresonance. The corresponding load dynamic responses for each substation are depicted in Figure 8, with the associated current dynamics presented in Figure 9. Finally, Figure 10 captures the dynamic responses in the fundamental ferroresonance mode, marking the onset of ferroresonance across all analyzed voltages and currents for the respective substations.

Table 10: Effect of Varying Loading Parameters for the Respective Substations

Loading Parameter Change	Substation	Peak Voltage Before Switch Opening (kV)	Peak Voltage After Switch Opening (kV)	Peak Current Before Switch Opening (A)	Peak Current After Switch Opening (A)	Voltage THD (%)	Current THD (%)
Baseline	Lafia Substation	0.415	0.400	27	33	2.5%	3.2%
R increased by 10%	Lafia Substation	0.415	0.415	27	31	2.3%	2.8%
R decreased by 10%	Lafia Substation	0.415	0.440	27	36	3.0%	4.1%
X increased by 10%	Lafia Substation	0.415	0.420	27	32	2.4%	3.0%
X decreased by 10%	Lafia Substation	0.415	0.430	27	39	3.1%	3.7%
R & X increased by 10%	Lafia Substation	0.415	0.415	27	33	2.2%	2.9%
R & X decreased by 10%	Lafia Substation	0.415	0.850	27	41	5.8%	6.5%
Baseline	Akwanga Subst.	0.415	0.415	27	32	2.7%	3.4%
R increased by 10%	Akwanga Subst.	0.415	0.410	27	30	2.3%	3.1%
R decreased by 10%	Akwanga Subst.	0.415	0.435	27	34	3.3%	4.2%
X increased by 10%	Akwanga Subst.	0.415	0.420	27	31	2.6%	3.2%
X decreased by 10%	Akwanga Subst.	0.415	0.425	27	36	3.5%	4.0%
R & X increased by 10%	Akwanga Subst.	0.415	0.400	27	31	2.1%	2.7%
R & X decreased by 10%	Akwanga Subst.	0.415	0.900	27	37	6.1%	7.0%
Baseline	Keffi Substation	0.415	0.420	27	31	2.9%	3.6%
R increased by 10%	Keffi Substation	0.415	0.420	27	29	2.5%	3.3%

UNDER PEER REVIEW

R decreased by 10%	Keffi Substation	0.415	0.435	27	33	3.7%	4.4%
X increased by 10%	Keffi Substation	0.415	0.425	27	28	2.8%	3.4%
X decreased by 10%	Keffi Substation	0.415	0.430	27	35	3.9%	4.6%
R & X increased by 10%	Keffi Substation	0.415	0.410	27	30	2.4%	3.2%
R & X decreased by 10%	Keffi Substation	0.415	0.950	27	36	6.4%	7.2%

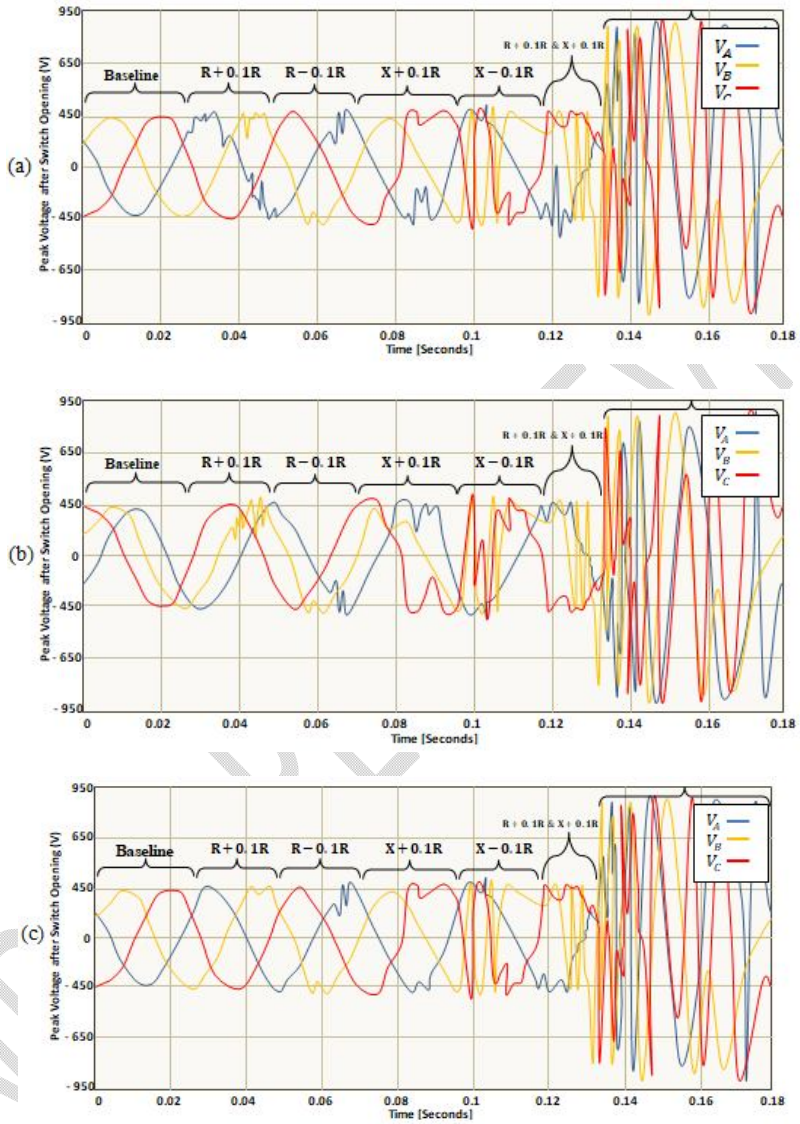

Figure 8: Baseline Transformer Voltage Responses for Varying Load Parameters for all the Substations; (a) Lafia; (b) Akwanga; and (c) Keffi

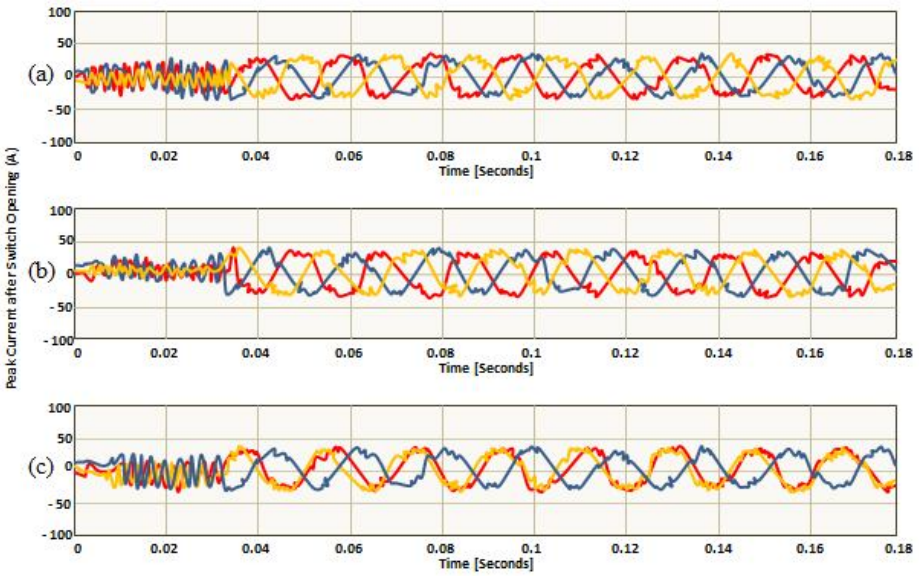

Figure 9: Baseline Transformer Current Responses for Varying Load Parameters for all the Substations; (a) Lafia; (b) Akwanga; and (c) Keffi

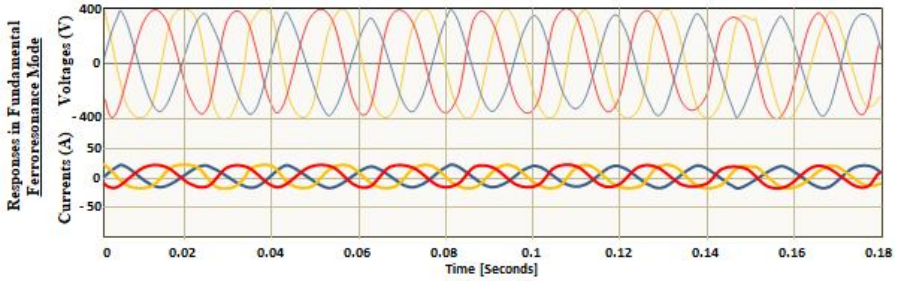

Figure 10: Dynamic Responses in the Fundamental Ferroresonance Mode, for all Analyzed Voltages and Currents for all Respective Substations

Table 11: Comparative Summary of Current Study Findings with Previous studies

Author	**Percentage Ferroresonance Mitigation**
Current Study	52% reduction
Shemshadi&Khorampour [15]	47% reduction
Gokhale et al. [12]	30%. reduction
Nene [11]	35% reduction
Chen et al. [19]	40% reduction
Zirka et al. [16]	28% reduction
Olguín-Becerril et al. [18]	50% reduction

4. DISCUSSION

Transformer behavior under varying conditions showed that core saturation, harmonic distortions, non-linear inductance, and load type/voltage variations significantly affect ferroresonance risk. This aligns with Shemshadi and Khorampour [15], who emphasized managing core saturation and inductance for ferroresonance mitigation. It also aligns with Gokhale et al. [12], who proposed load balancing in single-phase transformers to prevent ferroresonance.

At low voltages (50V, 100V), the transformer operated efficiently, with minimal magnetizing current and losses, indicating low ferroresonance risk, similar to Nene [11] on CCS in rural electrification; and Bini *et al*. [17] respectively who both found that reducing core loss resistance can dampen ferroresonance.

However, as voltage increased (200V-500V), magnetizing current and core losses rose, deepening core saturation and increasing ferroresonance risk, similar to Chen *et al.* [19], who identified voltage-driven ferroresonance modes. The Delta configuration (1.12Ω) had a lower risk than the Star-Grounded configuration (1.53Ω), in line with Zirka*et al.* [16]. Grading capacitance plays a critical role in resonance buildup. Increasing capacitance from 90 pF to 1550 pF significantly raised peak voltage and current, as observed in Lafia, where voltage rose from 0.420 kV to 2.400 kV, and current increased from 28A to 103A. Higher capacitance increases the energy stored in the system, thereby amplifying voltage and current oscillations during switching, which enhances ferroresonance risks. These findings reinforce Olguín-Becerril *et al.* [18], who highlighted the importance of capacitance management to control resonance phenomena.

Lower-order harmonics, particularly the 3rd (0.5A, 15V), strongly influence non-linear inductance, driving the resonance phenomenon. These harmonics can cause significant flux distortion, leading to an increase in core losses and deepening core saturation. Shemshadi and Khorampour [15] pointed out the necessity of harmonic filtering in reducing ferroresonance risks. Findings also reveal that implementing harmonic filtering technologies in transformers prone to ferroresonance could mitigate the impact of these lower-order harmonics by up to 52%, preventing excessive resonance buildup and enhancing transformer stability; which is in line with the findings of Nene [11]; and Chen *et al.* [19]. These trends underscore the need for careful management of grading capacitance and harmonic content, as well as the potential benefits of harmonic filtering, in line with studies from Olguín-Becerril et al. [18] and others. A comparative summary is presented in Table 11; of related literature with current study on the assessment of ferroresonance and its effects in distribution networks.

5. CONCLUSION

This study assessed ferroresonance susceptibility in distribution transformers, examining core saturation, harmonic distortions, and the effects of grading capacitance. Findings revealed that elevated voltage and load conditions significantly increased core losses and magnetizing currents, amplifying the risk of ferroresonance. Delta configurations exhibited a lower risk compared to Star-Grounded configurations, underscoring the role of winding type in ferroresonance resilience. Managing harmonic distortion through filtering and strategic winding configuration emerged as essential; excessive grading capacitance was shown to elevate peak voltage, current, and Total Harmonic Distortion (THD), thereby exacerbating resonance risks. By highlighting the influence of transformer design parameters, particularly core material properties and harmonic filtering, this study provides valuable insights for improving ferroresonance resilience in low-voltage distribution systems. Practically, it emphasizes the need for careful transformer design to mitigate risks and improve resilience, enhancing power quality in sensitive substations. Effective management of grading capacitance and harmonic distortion proved essential in preventing operational disruptions, contributing to more stable distribution networks.

While this study offers critical findings, it was limited to laboratory tests, with real-world variables like transformer model variations potentially impacting ferroresonance behavior. Future research should explore different transformer models, configurations, and advanced mitigation strategies, including adaptive control systems. Additionally, integrating diverse field data with machine learning-based models could refine ferroresonance risk assessments, leading to more robust prediction and prevention methods in varied substation environments.

Disclaimer (Artificial intelligence)

Author(s) hereby declare that NO generative AI technologies such as Large Language Models (ChatGPT, COPILOT, etc.) and text-to-image generators have been used during the writing or editing of this manuscript.

REFERENCES

[1] Valverde, V., Mazón, A.J., Zamora, I. &Buigues, G. (2007). Ferroresonance in Voltage Transformers: Analysis and Simulations. *Renewable Energy and Power Quality Journal (RE&PQJ)*, 1(5). doi:10.24084/repqj05.317.

[2] Engdahl, G. (2017). Ferroresonance in Power Systems: Literature Study. *Energiforsk AB* (Accessed online). Retrieved from: https://energiforskmedia.blob.core.windows.net/media/23470/ferroresonance.

[3] Cetina R., Madrigal-Martínez, M., Torres-García, V. & Corona-Sánchez, M. (2021). Ferroresonance Simulations in Radial Systems using ATPDraw. *ECORFAN Journal-Taiwan*, 5(10), 1-10. https://doi.org/10.35429/EJT.2021.10.5.1.10.

[4] Swain, A., Abdellatif, E., Mousa, A. & Pong, P.W.T. (2022). Sensor Technologies for Transmission and Distribution Systems: A Review of the Latest Developments. *Energies*, 15(19), 1 – 37. https://doi.org/10.3390/en15197339.

[5] Kutija, M. &Pravica, L. (2021). Effect of Harmonics on Ferroresonance in Low Voltage Power Factor Correction System - A Case Study. *Applied Sciences*, 11(10), 1-20. https://doi.org/10.3390/app11104322.

[6] Abdul-Malek, Z., Mehranzamir, K., Salimi, B., Afrouzi, H., Afrouzi, A. & Mashak, S. (2013). Investigation of Ferroresonance Mitigation Techniques in Voltage Transformer Using ATP-EMTP Simulation. *JurnalTeknologi*, 64(4), 85-95. https://doi.org/10.11113/jt.v64.2107.

[7] Abdullahi, J. & Abdulhamid, A. A. (2024). Optimized Design of a 50kVA Transformer for Ferroresonance Mitigation and Power Quality Enhancement. *International Journal of Innovative Science and Research Technology*, 9(5), 1455. https://doi.org/10.38124/ijisrt/IJISRT24MAY479.

[8] Tarko R, Nowak W, Gajdzica J, Czapp S. Analysis of Ferroresonance Mitigation Effectiveness in Auxiliary Power Systems of High-Voltage Substations. Energies. 2024 May 18;17(10):2423.

[9] Nene SW. Mathematical Modeling of Multiple Capacitor Coupled Substations (CCS) Impact on Transmission Lines and Approaches for Ferroresonance Suppression. Open Journal of Modelling and Simulation. 2024 Oct 21;12(4):101-13.

[10] Temiz, İ. & Tarkan, N. (2024). Ferroresonance phenomena in power systems. Journal of Mechatronics and Artificial Intelligence in Engineering, 5(1), 1-8. https://doi.org/10.21595/jmai.2023.23810.

[11] Nene, S. W. (2024). Mathematical modeling of multiple capacitor coupled substations (CCS) impact on transmission lines and approaches for ferroresonance suppression. Open Journal of Modelling and Simulation, 12(4), 101–113. https://doi.org/10.4236/ojmsi.2024.124007.

[12] Tovbaev, A., Ibadullayev, M. &Davronova, M. (2024). Study of subharmonic oscillation processes in ferroresonance circuits. E3S Web of Conferences, 525, 03008. https://doi.org/10.1051/e3sconf/202452503008.

[13] Begmatov, S. E. (2024). Ferroresonance in three-phase electrical networks. Technical Science and Innovation, 2024(2), Article 11. https://doi.org/10.XXX/tsin.2024.XXX.

UNDER PEER REVIEW

[14] Gokhale, G. S., Mork, B. A., O'Donnell Jr, J. & Brehmer, S. R. (2023). Ferroresonance case study in a distribution network and the potential impact of DERs and CVR/VVO. Electric Power Systems Research, 220, 109303. https://doi.org/10.1016/j.epsr.2023.109303.

[15] Shemshadi, A. &Khorampour, P. (2022). The Investigation of Ferroresonance Voltage Fluctuation Considering Load Types and Damping Factors. *Energy Harvesting and Systems*. https://doi.org/10.1515/ehs-2022-0002.

[16]Zirka, S. E., Moroz, Y. I., Zhuykov, A. V., Matveev, D. A.,Kubatkin, M. A., Frolov, M. V.& Popov, M. (2021). Eliminating VT Uncertainties in Modeling Ferroresonance Phenomena Caused by Single Phase-to-Ground Faults in Isolated Neutral Network. *International Journal of Electrical Power & Energy Systems*, 133, 107275. https://doi.org/10.1016/j.ijepes.2021.107275.

[17] Bini, M.S.H., Ang, S. P., Yeo, K. S. K., Khalil, A.& Jaafar, S. (2020). Analytical Prediction of Initiation of Ferroresonance Modes. *Journal of Physics: Conference Series*, 1529, 032087. https://doi.org/10.1088/1742-6596/1529/3/032087.

[18] Olguín-Becerril, M. A., Angeles-Camacho, C.& Fuerte-Esquivel, C. R. (2014). Ferroresonance in Subharmonic 3rd Mode in an Inductive Voltage Transformer: A Real Case Analysis. *Electrical Power and Energy Systems, 61, 318-325*. https://doi.org/10.1016/j.ijepes.2014.03.057.

[19] Chen, X., Caputo, J.-P.&Baghzouz, Y. (2012). Harmonic Analysis of Ferroresonance in Single-Phase Transformers. In *2012 IEEE 15th International Conference on Harmonics and Quality of Power (pp. 535-540). Hong Kong, China.*https://doi.org/10.1109/ICHQP.2012.6381277.

[20] Behdani, B., Allahbakhshi, M. &Tajdinian, M. (2021). On the Impact of Geomagnetically Induced Currents in Driving Series Capacitor Compensated Power Systems to Ferroresonance. *International Journal of Electrical Power & Energy Systems*, 125 (2), 106424. https://doi.org/10.1016/j.ijepes.2020.106424.

[21] Rezaei, S. (2019). Power Oscillation Due to Ferroresonance and Subsynchronous Resonance. In *IntechOpen* (pp. 1-21). https://doi.org/10.5772/intechopen.81724.

[22] Majka, Ł. & Klimas, M. (2019). Diagnostic approach in assessment of a ferroresonant circuit. *Electrical Engineering*, 101 (2019), 149–164. https://doi.org/10.1007/s00202-019-007615.

[23] Begmatov, S.E., Khalbutaeva, K.I. &Dusmukhamedova, S.A. (2020). Study of Ferroresonance in Electric Networks Taking into Account the Generalized Model of Nonlinear Inductance. *In Rudenko International Web Conference on Methodological Problems in Reliability Study of Large Energy Systems (RSES 2020), 216 (01115), Sofia, Bulgaria.* 20-23. doi:10.1051/e3sconf/202021601115.

[24] Hoshimov, F.A., Bakhadirov, I.I., Erejepov, M. &Djumamuratov, B. (2019). Development of Method for Normalizing Electricity Consumption. *In Rudenko International Conference on Methodological Problems in Reliability Study of Large Energy Systems (RSES 2019), 139 (01074)*. doi:10.1051/e3sconf/201913901074.

[25] Mullins, E. (1991). Recent Developments in Quality Control: An Introduction to Taguchi methods. *Nigerian Journal of Technology (NIJOTECH), 15(1), 1-15*.

UNDER PEER REVIEW